AIP | Review of Scientific Instruments

Four-dimensional (4D) tracking of high-temperature microparticles

Zhehui Wang, Q. Liu, W. Waganaar, J. Fontanese, D. James, and T. Munsat

Citation: Review of Scientific Instruments **87**, 11D601 (2016); doi: 10.1063/1.4955280
View online: http://dx.doi.org/10.1063/1.4955280
View Table of Contents: http://scitation.aip.org/content/aip/journal/rsi/87/11?ver=pdfcov
Published by the AIP Publishing

Four-dimensional (4D) tracking of high-temperature microparticles

Zhehui Wang,[1,a)] Q. Liu,[1] W. Waganaar,[1] J. Fontanese,[2] D. James,[2] and T. Munsat[2]
[1]*Los Alamos National Laboratory, Los Alamos, New Mexico 87545, USA*
[2]*University of Colorado, Boulder, Colorado 80309, USA*

(Presented 6 June 2016; received 4 June 2016; accepted 14 June 2016; published online 8 July 2016)

High-speed tracking of hot and molten microparticles in motion provides rich information about burning plasmas in magnetic fusion. An exploding-wire apparatus is used to produce moving high-temperature metallic microparticles and to develop four-dimensional (4D) or time-resolved 3D particle tracking techniques. The pinhole camera model and algorithms developed for computer vision are used for scene calibration and 4D reconstructions. 3D positions and velocities are then derived for different microparticles. Velocity resolution approaches 0.1 m/s by using the local constant velocity approximation. *Published by AIP Publishing.* [http://dx.doi.org/10.1063/1.4955280]

I. INTRODUCTION

There has been growing interest in diagnostics, understanding, and applications of particulates with sizes ranging from sub-microns to above millimeters in magnetic fusion.[1] Plasma-material interactions due to edge-localized modes (ELMs), exhaust to divertors and transients such as disruptions can produce, in addition to electrons, ions and atoms, hot and molten dust or microparticles. The energy required to produce a 10-μm diameter tungsten dust particle, for example, is less than 5×10^{-4} of the energy needed to produce the atomic tungsten vapor of comparable mass and as a result, the potential plasma core contamination due to tungsten particulates could be more significant than tungsten vapor. High-speed tracking using imaging cameras is a natural choice in studying these objects *in situ*. Furthermore, such measurements provide rich information about the magnetic fusion environment, including the properties of microparticles, the high-temperature plasmas, and their mutual interactions. The information can also aid technological development related to plasma fueling, ELM pacing, wall conditioning, and disruption mitigation. Another interest comes from modeling and simulations which need experimental data to validate physics and computational approximations.

We report recent results of time-resolved three-dimensional (3D) and therefore "4D" microparticle tracking diagnostics. Computational algorithms developed for computer vision have been adopted for scene reconstruction and particle velocity measurements.[2–5] An exploding-wire microparticle source is used to create high-temperature microparticles of different sizes and velocities, which have been conveniently collected for microscopic analysis following the tracking measurements.

II. PRINCIPLE AND SETUP FOR PARTICLE TRACKING

As in computer vision, each camera aperture is approximated by a pinhole. At any instant in time, a point M in 3D real space is projected onto a pixel point m through the aperture, commonly called the optical center C in the pinhole camera model, as shown in Fig. 1, where the subscript "l" is for the left camera and "r" for the right. The point M, together with the two optical centers C_l and C_r, forms a plane that both projections m_l and m_r reside on. The projection geometry is also known as the epipolar geometry. The projections of the optical centers are e_l and e_r, called epipoles, are independent of M. Furthermore, once m_l (m_r) is given, the corresponding m_r (m_l) resides on a line that always passes through e_r (e_l). The two lines are called epilines for each M.

Mathematically, the homogeneous coordinates of $\tilde{M}$ (X, Y, Z, 1) are linearly related to the homogeneous pixel coordinates $\tilde{m}$ (u, v, 1) through

$$\tilde{s}_{l,r}\tilde{m}_{l,r}^{T} = \tilde{\mathbf{P}}_{l,r}\tilde{M}^{T}, \tag{1}$$

where the superscript "T" is for transpose matrix operation. The left and right projection matrices $\tilde{\mathbf{P}}_l$ and $\tilde{\mathbf{P}}_r$ given in the same form,[4,5]

$$\tilde{\mathbf{P}} = \mathbf{AB} \equiv \begin{bmatrix} f/p_u & gf/p_v & u_0 \\ 0 & f/p_v & v_0 \\ 0 & 0 & 1 \end{bmatrix} \begin{bmatrix} R_{11} & R_{12} & R_{13} & t_1 \\ R_{21} & R_{22} & R_{23} & t_2 \\ R_{31} & R_{32} & R_{33} & t_3 \end{bmatrix}, \tag{2}$$

where $\mathbf{A}$, a 3×3 matrix is determined by the intrinsic parameters: f the focal length, p_u, p_v the size of each pixel in the horizontal and vertical directions, and u_0, v_0, the pixel coordinates of the optical axis. The 3×4 matrix $\mathbf{B}$ is determined by a 3×3 rotation matrix $\mathbf{R} \equiv [R_{ij}]$ and a translation vector $\mathbf{T} = (t_1, t_2, t_3)$ from one optical center to the other.

Camera calibration is to derive the matrix elements from the images of calibration objects and their relative positions. We used two Vision Research phantom v2511 cameras ($p_u = p_v = 28$ μm). The frame rate was fixed at 100 kfps with an image size of 384×384 pixels. TEMA software by

Note: Contributed paper, published as part of the Proceedings of the 21st Topical Conference on High-Temperature Plasma Diagnostics, Madison, Wisconsin, USA, June 2016.

a)Author to whom correspondence should be addressed. Electronic mail: zwang@lanl.gov

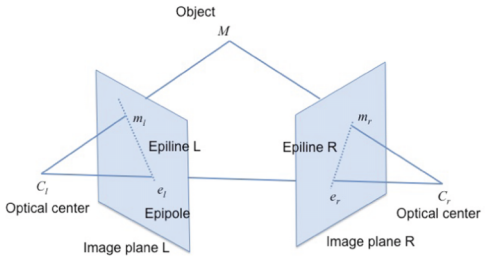

FIG. 1. Epipolar geometry for two camera views in the pinhole model. Epipoles are the two intersections of the line of the optical centers C_l and C_r with the two image planes. The epipolar plane is formed out of C_l, C_r and the object M.

Specialised Imaging was used in calibration. The focal lengths f_l, f_r were 56.19 mm and 55.49 mm, respectively. The left optical center C_l was at (181.5, 211.7) in pixel coordinates. C_r was (147.0, 228.6). The 3D coordinates of C_r were chosen to be at ($X_r = 0$, $Y_r = 0$, $Z_r = 0$). The translation vector for the left camera $\mathbf{T} = (56.72, 0.133, -35.07)$ cm. The exposure time was 2 μs for each image frame.

III. RESULTS AND DISCUSSION

We built an exploding-wire apparatus to generate high-temperature microparticles. The particles were collected in ethanol for analysis by an optical microscope. One example is shown in Fig. 2. The nearly spherical shapes and smooth surfaces confirm the existence of a hot and molten state prior to cooling down in ethanol.

A few frames of the wire-explosion movie by each camera are shown in Fig. 3, where the left column is from the left camera and the right column is from the right camera. The time-integrated images at the bottom (after background removal) can be regarded as the 4D tracks projected onto two 2D image planes.

For 3D scene reconstruction at any instant in time, it is necessary to correlate tracks in the two camera views. In addition to using the static objects and time-independent features in the background, we found that the changes in the brightness of microparticle incandescence can be used for track pairing. One example is shown in Fig. 4, where two

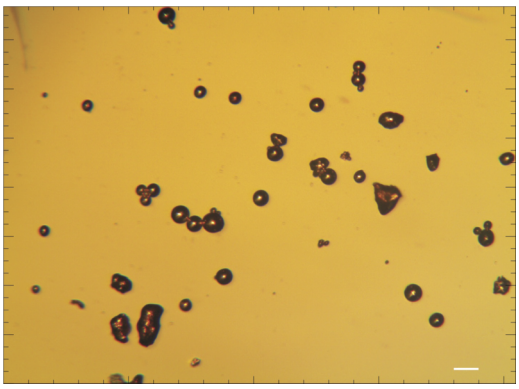

FIG. 2. A copper microparticle sample under an optical microscope (scale bar = 50 μm). The wire diameter was 260 μm. The median particle diameter was about 25 μm.

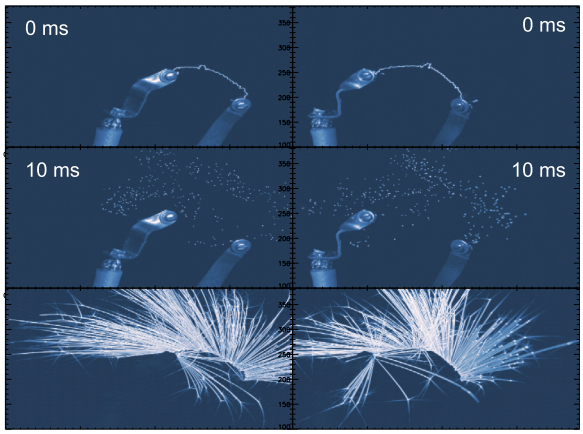

FIG. 3. The top two images show the initiation of a wire explosion. The middle two frames are the cloud of microparticles at 10 ms into explosion. The bottom two images are the time-integrated image of the full explosion process by superimposing the whole movie sequences over each other.

thick tracks (shown together with other tracks as background) were identified to be the same particle track because both peaked in brightness at around 22 ms. Most tracks typically have different temporal dependence in brightness. Using the peak coincidence as a pairing criterion greatly reduces the number of possible matches, even when several tracks may be present simultaneously.

Further validation of track pairing is through the so-called fundamental matrix **F**, which is derived from the matrices **A**, **R** and **T** mentioned above. Specifically, for each pair of points $\tilde{m}_l(u_l, v_l, 1)$ and $\tilde{m}_r(u_r, v_r, 1)$ in homogeneous coordinates, the epipolar constraint requires that $\tilde{m}_r \mathbf{F} \tilde{m}_l^T = 0$. Examples of epipolar constraint checks are shown in Fig. 5. The position of a point in the left camera gives rise to the epiline in the right cam that the matched point should reside on, and vice versa.

A. 3D coordinates calculation

After track pairing, triangulation is then used to determine a point's 3D position from the two corresponding pixel locations. The accuracy is compromised by measurement

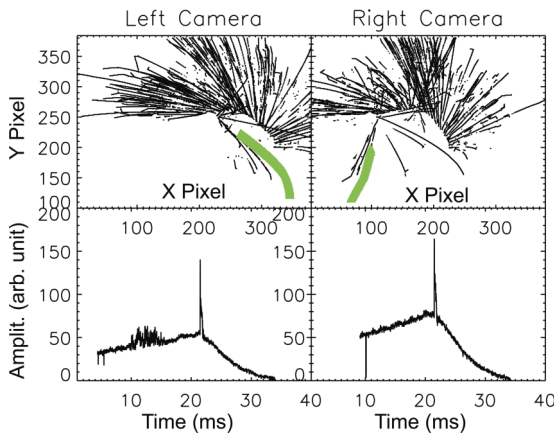

FIG. 4. Pairing of left and right particle trajectories through the incandescence peak timing. The two thick tracks (top) are confirmed to be the same particle trajectory because of the coincidence in the timing of the peak brightness (bottom).

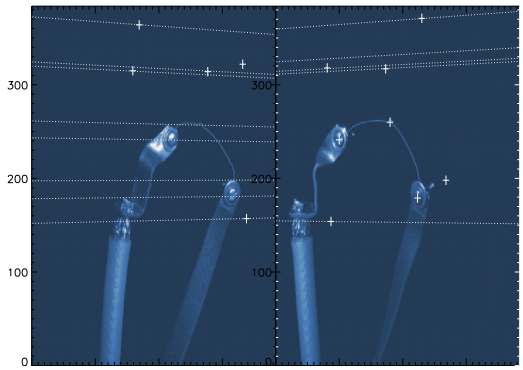

FIG. 5. Validation of the camera matrices, as well as track-pairing algorithm using the epipolar constraint. More details are given in the text.

and systematic errors such as lens aberration, finite pixel size, and noise. Several "optimal intersection" algorithms have been described previously.[6] The results for the track highlighted in Fig. 4 are shown in Fig. 6 using two of them: the linear least-square method and the 6° non-iterative polynomial method. The indistinguishable overlap of the two results shows essentially no difference from the two approaches.

B. Velocity measurement

Following the 3D position calculations, the 3D velocities are deduced from the time derivatives, $\mathbf{v}(t) = [\dot{x}(t), \dot{y}(t), \dot{z}(t)]$, where $\dot{x}(t)$ symbolizes the time derivative of the x coordinate with respect to time and so forth. In digital cameras, both time and position are discretized, leading to an artificial digital noise in velocity as large as

$$\delta v_p = \frac{2l_p}{\delta t_p}, \tag{3}$$

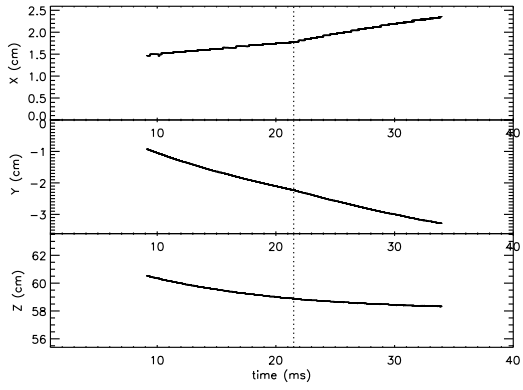

FIG. 6. Reconstructed temporal evolution of the 3D track of the microparticle highlighted in Fig. 4. Two triangulation algorithms, least square, and 6° polynomial give essentially the same answer. The vertical dashed line corresponds to the timing of the peak incandescent intensity.

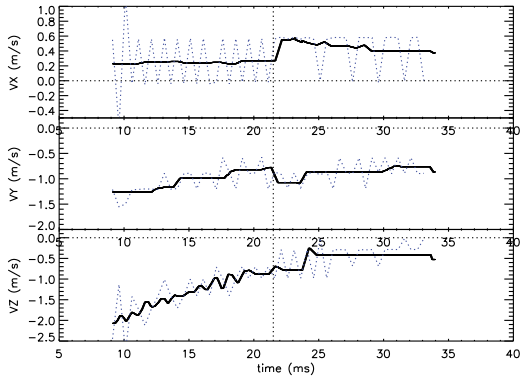

FIG. 7. Velocity derived as a function of time for the trajectory in Fig. 6. The "constant local velocity" approximation (solid lines) reduces the velocity artifacts due to the finite pixel size (dashed lines).

which in the current case, $l_p = 28$ μm is the pixel size and $\delta t_p = 10$ μs is the frame-to-frame time. Therefore the velocity noise due to discreteness can be as large as 5.6 m/s or a "digital noise" for acceleration as large as 5.6×10^5 m/s^2. To reduce the effects of digital noise, a time average over multiple frames is needed. The dashed lines in Fig. 7 are for averages over 50 frames or 0.5 ms in real time. The equivalent noise reduction is less than $\delta v_p/N_p$ for N_p frames. We also used the constant local velocity assumption to further reduce the velocity fluctuations, which reduced artifacts in velocity calculations.

In summary, we report hardware and software development for 4D high-temperature microparticle tracking, which can be applied to different magnetic fusion scenarios. This work paves the way towards force measurement (acceleration) of these objects.

ACKNOWLEDGMENTS

We thank Mr. Phiroze Dalal (Vision Research), Mr. Robin Nicholai, Mr. Chris Tenney (both from Specialised Imaging Inc.), Dr. Magnus Olsson (Image Systems AB) for help and/or discussions about the development, and Dr. Don Rej (LANL) for encouragement to carry out the work, which is supported by the US DoE/Fusion Energy Sciences program.

[1]Z. Wang, R. Lunsford, D. K. Mansfield, and J. H. Nichols, J. Plasma Phys. **82**, 615820202 (2016).
[2]Q.-T. Luong and O. D. Faugeras, Int. J. Comp. Vis. **17**, 43-75 (1996).
[3]R. I. Hartley and A. Zisserman, *Multiple View Geometry in Computer Vision*, 2nd ed. (Cambridge, 2004).
[4]S. J. D. Prince, *Computer Vision: Models, Learning and Inference* (Cambridge, 2012).
[5]Z. Zhang, R. Deriche, O. D. Faugeras, and Q.-T. Luong, Artif. Intell. **78**, 87-119 (1995).
[6]R. I. Hartley and P. Sturm, "Triangulation," Comput. Vision Image Understanding **68**(2), 146-157 (1997).